# Interaction of hydrogen with the bulk, surface and subsurface of crystalline RuO2 from first principles

Ankita Jadon, Carole Rossi, Mehdi Djafari-Rouhani, Alain Estève, David Pech

Physics Open 7 (2021) 100059

Contents lists available at ScienceDirect

Physics Open

journal homepage: www.journals.elsevier.com/physics-open

# Interaction of hydrogen with the bulk, surface and subsurface of crystalline $RuO_2$ from first principles

Ankita Jadon **, Carole Rossi, Mehdi Djafari-Rouhani, Alain Estève *, David Pech

*LAAS-CNRS, Université de Toulouse, CNRS, Toulouse, France*

ARTICLE INFO

*Keywords:*
$RuO_2$
Pseudocapacitor
DFT
Ab initio
Diffusion of protons
Electrochemistry

ABSTRACT

Hydrogen and its interaction with metal oxide surfaces is of major importance for a wide range of research and applied fields spanning from catalysis, energy storage, microelectronics, to metallurgy. This paper reviews state of the art of first principles calculations on the well-known ruthenium oxide ($RuO_2$) surface in its (110) orientation and its interaction with hydrogen. In addition to it, the paper also fills gaps in knowledge with new calculations and results on the (001) surface. Bulk and surface interactions are thoroughly reviewed. This includes systematic analysis of adsorption sites, local agglomeration propensity of hydrogen, and migration pathways in which literature data and their potential deviations are explained. We notably discuss novel results on propensity for agglomeration of hydrogen within bulk channels [001] oriented in which the proton-like behavior of adsorbed hydrogen hinders further agglomeration in adjacent channels. The paper brings new insights into the migration pathways on the surface and in bulk, both exhibiting preferential diffusion paths along the [001] direction. The paper finally investigates the subsurface region. We show that while the subsurface has more stable sites for adsorption compared to bulk, its accessibility from the surface shows prohibitive activation barriers inhibiting penetration into subsurface and bulk. We further calculate and discuss adsorption and penetration processes on the alternative $RuO_2$ (001) surface.

## 1. Introduction

In addition to its important role in heterogeneous catalysis, $RuO_2$ exhibits a stable and well ordered surface, $RuO_2$ (110), establishing itself as a good model system for studying catalytic as well as electrochemical processes, both experimentally and theoretically [1–8]. Among gas or liquid chemical species to put in contact with, hydrogen is attracting considerable attention due to its role in a collection of different applications, including production of green energy [9] corrosion [10], sensing [11,12], fuel cells [13,14] and electrochemical capacitors [6,15,16], to name a few. The latter is one particularly interesting example since the basic chemical interaction is not restricted to the surface only, and its spatial extension to the subsurface and bulk is neither documented by first principles calculations such as Density Functional Theory (DFT), nor well understood or quantified experimentally. Electrochemical capacitors, contrary to batteries, which require bulk phase transformations, are driven by much faster reversible surface and subsurface chemical reactions with higher degree of non destructive cyclability based on the charging and discharging of hydrogen atoms. To this respect, understanding with an atomic scale precision the kinetics and occurrence of these reactions is a crucial challenge to design the next generation of capacitors with enhancement of both energy and power densities. The penetration of hydrogen into the subsurface or even deeper penetration into the electrode is also critical. While impedance spectroscopy measurements can provide a crude estimate of the surface versus inward hydrogen location, only atomic scale modelling can precisely render how and where penetration process becomes feasible as a function of the electrode nanostructure. This point has never been addressed from a theoretical perspective: what characterizes the intermediate subsurface reaction zone, its reactivity and spatial extension facing hydrogen exposure. Concerning surface interactions, DFT studies in literature have concentrated on the interaction of water with the stable $RuO_2$ (110) surface for electrochemical purposes, related to water splitting mechanisms or more generally, heterogeneous reactions [4,8,17–19]. In this scope, most of the literature is focused on hydrogen interacting with the $RuO_2$ (110) surface using combined experimental (including temperature programmed desorption and STM experiments) and theoretical approaches, to picture the molecular and dissociative behavior of

* Corresponding author.
** Corresponding author.
*E-mail addresses:* ajadon@laas.fr (A. Jadon), aesteve@laas.fr (A. Estève).

https://doi.org/10.1016/j.physo.2021.100059
Received 28 July 2020; Received in revised form 16 December 2020; Accepted 16 January 2021
Available online 21 February 2021

di-hydrogen on the surface [17,18,20–24]. A propensity for dissociation and stabilization of hydroxyl groups on the bridging oxygen sites of the $RuO_2$ (110) has been observed [7,25]. A similar study has been performed on an oxygen rich surface showing similar tendency to form hydroxyl species, the paper also reports on migration energies of hydrogen on the surface [7,26]. While nothing has been reported so far on the penetration and reaction of hydrogen into the subsurface, very few publications have investigated bulk properties. Kim et al. [27] have investigated the behavior of hydrogen into perfect and defective bulk $RuO_2$. In the specific context of supercapacitors, where hydrous $RuO_2$ is commonly used experimentally, the seminal work by V. Ozolins et al. [28] addresses a number of issues related to hydrogen in crystalline $RuO_2$ as well as proposing new directions to investigate the more complex case of hydrous material. Jadon et al have shown that migration pathways are energetically favorable along the [001] direction, leading to a deeper $H^+$ penetration within the bulk of the active material and a much higher charge storage ability[29]. In conclusion, the overall literature on the basic mechanisms controlling the interaction of hydrogen with the surface and bulk $RuO_2$ is rather sparse and incomplete: the interaction of hydrogen with bulk is poorly documented; on the surface, there is still debate on the kinetics of di-hydrogen dissociation at very low temperature [17]. In this context, we aim at providing a rationale of the behavior of hydrogen atoms in interaction with $RuO_2$: surface, and bulk, with complementary focus on hydrogen migrations pathways and agglomeration propensity. We will also discuss the intermediate subsurface region, in which we will detail penetration pathways to understand why the measured pseudocapacitance level is poor when considering crystalline $RuO_2$. As a result, we will provide new routes to enhance hydrogen agglomeration on crystalline $RuO_2$ surfaces. We believe this work will provide a basic reference to further address more complex $RuO_2$ model-systems, such as hydrous $RuO_2$ ($RuO_2.xH_2O$).

## 2. Computational details

In this study, the DFT-based Vienna ab initio simulation package (VASP) was employed to perform calculations [30,31], using Perdew, Burke, and Ernzerhof (PBE) method for treating exchange and correlation. The valence electrons were described with a planewave basis set, with an optimized cut-off energy of 400 eV [32,33]. Nuclei and core electrons were treated with pseudopotentials of the projector augmented wave type. To improve the description of the long-range interactions, the DFT-D3 method of Grimme as implemented in VASP was employed [34]. The Kohn-Sham equations were solved self-consistently until the energy difference between cycles becomes lower than $10^{-4}$ eV. Methfessel-Paxton smearing with $\sigma = 0.1$ eV was used [35].

The ionic positions were optimized until all forces were smaller than 0.05 eV/Å per atom; this parameter was set after carrying out a convergence test for the forces.

The bulk $RuO_2$ was optimized from its tetragonal phase, with experimental crystal lattice parameters: a = 4.51 Å and c = 3.11 Å. Using a 6 × 9 × 6 mesh of k-points, we found optimized values of a = 4.47 Å and c = 3.08 Å. From this unit-cell, we built an extended bulk and a (110) surface (see Fig. 1) to study hydrogen adsorption, migration, agglomeration, and penetration, with the following properties:

1. The bulk $RuO_2$ was built by first reorienting the crystal axes in the three [1 1 0] [1–10], and [0 0 1] directions, in order to construct the (110) surface by simply cleaving this bulk $RuO_2$ across a parallelepiped face. The elementary cell is no more primitive, with parameters $a\sqrt{2}$ and c. This elementary cell is then multiplied by (2 × 2 × 4), ending up with an almost cubic cell of 12.65 Å × 12.65 Å × 12.33 Å. The total number of atoms in this cell amounts to 64 Ru and 128 oxygen atoms. When inserting hydrogen atoms, the bulk supercell volume and shape were kept constant to their pure $RuO_2$ converged values to mimic the constraint imposed by crystalline $RuO_2$. Periodic boundary conditions are then applied in all three directions to construct a large cell where all DFT calculations are carried out with only a gamma centered k-point mesh.
2. The surface model was built from a slab composed of a total of four layers of $RuO_2$, each containing 16 Ru and 32 oxygen atoms. The two bottom layers were kept fixed in their bulk positions, during all energy minimization procedures, to mimic bulk effects. A vacuum space of 15 Å was added on top of the (110) surface and periodic boundary conditions were applied to this unit cell in all three dimensions. Following a TEM experimental study, followed by a number of DFT-based investigations of the $RuO_2$ (110) surface, only bridging oxygens were kept on top of the surface Ru atoms [4,17,36]. To this respect, the surface consists of 32 atoms in total out of which eight are bridging oxygen ($O_{br}$), eight are ruthenium atoms and sixteen are planar oxygen ($O_{pl}$). This leaves unsaturated surface Ru atom rows. To compensate asymmetry of the slab between top and bottom surfaces, a linear dipole correction was added to the local potential as suggested in Refs. [37,38]. In addition, dangling bonds of Ru atoms in the bottom layer were saturated with H species. The total number of atoms in the unit cell amounts therefore to 200.

The Nudged Elastic Band (NEB) method was used to calculate migration barriers. All energies of hydrogen interacting with bulk or surface materials are calculated with respect to a reference energy: that of an isolated molecular hydrogen at an infinite position from ruthenium oxide. The adsorption energy of the hydrogen atom is expressed as the following equation (1).

$$E_{ads} = E_{RuO_2/H} - E_{cleanRuO_2} - 1/2E_{H_2} \quad (1)$$

Where $E_{RuO_2/H}$ is the total energy of a single hydrogen atom in the $RuO_2$

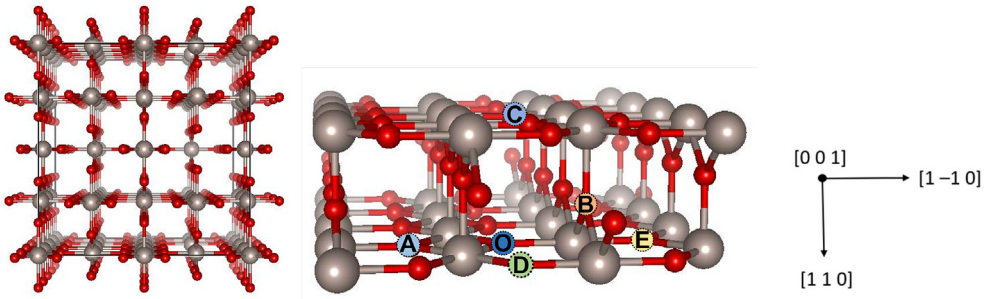


(a) a (b) b

**Fig. 1.** [a] A perspective view of $RuO_2$ showing the square channels along the [001] direction. Red: O; gray: Ru. [b] Possible neighboring sites for hydrogen migration in bulk $RuO_2$. The initial adsorbed hydrogen is shown in green and marked. (For interpretation of the references to colour in this figure legend, the reader is referred to the web version of this article.)

bulk on (110) surface, $E_{cleanRuO_2}$ the total energy of the bare bulk/surface and $E_{H_2}$ the total energy of the isolated hydrogen molecule.

## 3. Hydrogen in bulk $RuO_2$

This section focuses on bulk $RuO_2$ interacting with hydrogen. Two subsections investigate adsorption, agglomeration, and migration of hydrogen atoms. Moving on, the next two section will be dedicated to surface and subsurface interactions.

### 3.1. Adsorption and agglomeration of hydrogen in bulk $RuO_2$

In bulk $RuO_2$, all oxygen atoms are topologically equivalent, but moving along [001] direction, they alternate periodically between the two equivalent [110] and [1–10] orientations. Still, the hydrogen bond orientation with respect to its oxygen neighbors allows drawing two potential stable configurations. Both these initial configurations lead to a unique adsorption configuration shown in Figs. S1–a. Note that Fig. 1 shows perspective views of [001] channel that is a central entity in the $RuO_2$ structure, having clear square section and repeated units separated from each other by 3.16 Å. The adsorption energy of one hydrogen atom on oxygen is −0.11 eV and the O–H bond length is 1.00 Å, while the hydrogen bond with the neighboring oxygen atom at the opposite side of the channel, i.e. in the [110] direction, is 1.82 Å. Depending on the oxygen atom considered for adsorption, the OH axis is either [110] or [1–10] oriented. In terms of charge transfer after interaction, we note that hydrogen exhibits a drastic electronic loss. A Bader charge analysis was carried out as suggested by Henkelman et al. [39]. The analysis shows that the hydrogen atom becomes positively charged by +0.63 q (see Table 1, where q is the absolute value of the electron charge). This substantial charge transfer gives the hydrogen atom a proton like behavior in the overall neutral supercell. This amount of charge is transferred to the oxygen atom which is bonded to the hydrogen atom. The oxygen atom now acquires a charge of −1.54 q, compared to −0.83 q in crystalline $RuO_2$. Ru atoms bonded to the OH species have a charge of almost +2 q, meaning that they are even more depleted (by 0.3 q) after H adsorption. Charge transfers are reported in Table 1, where we show that they are not limited to first neighbors. Rather, a long-range behavior, compatible with macroscopic polarization effects is observed. Note that the gain, which is higher than the hydrogen contribution, can be explained by this macroscopic polarization. These findings agree well with the calculation by Ozolins and co-workers in Ref. [28] concerning perfect $RuO_2$ and the charge attributed to the hydrogen atom. Some deviations are noticed on charges on Ru and O, probably because of the small cell size utilized in their calculations and because their model system (called RuO–OH) deviates from the perfect $RuO_2$. As a result, the non local effects are not provided in their study. In Ref. [40], Kim and Lai, who consider a slightly smaller crystalline supercell, have very similar charge transfers compared to the present study on the bonded and non bonded oxygen atoms (0.55 q difference), and bonded Ru atom (+1.96 q). In order to study local hydrogen agglomeration, different configurations, shown in Fig. 2, are considered. The results are presented in Table 2.

**Table 1**
A comparison of Bader charge transfers for a perfect $RuO_2$ and $RuO_2$–H with data from literature. $Ru_b$: bonded Ru; $Ru_{nb}$: non-bonded Ru.

| Compound | Ion | Charge transfer | Ref. [15] |
|---|---|---|---|
| $RuO_2$ | Ru | +1.67 | +1.6 |
| | O | −0.83 | −0.8 |
| $RuO_2$–H | $Ru_b$ | +1.98 | +1.3 |
| | $Ru_{nb}$ | +2.04 | – |
| | $O_b$ | −1.54 | −1.0 |
| | $O_{nb}$ | −1.03 | −0.9 |
| | H | +0.63 | +0.6 |

Starting with two hydrogen atoms in bulk, occupying one every two oxygen atoms (6.13 Å apart), we calculated −0.17 eV energy per H atom, which is slightly higher than the adsorption energy of a single hydrogen atom (−0.11 eV). We note the attractive energy (0.12 eV), despite the strong electrostatic repulsion of charged hydrogen. If now hydrogen atoms are adsorbed on two neighboring oxygen atoms along the [001] direction, the energy slightly drops to −0.14 eV, still exhibiting attractive energy (0.06 eV), as compared to the single occupancy. The decrease in energy is due to the reduced H–H interatomic distance that drops to 3.13 Å. Other configurations (see Fig. 2, configurations [a] and [c] and Table 1) show relatively less thermodynamic stability to allow hydrogen agglomeration, particularly at room temperature, as they require closer distance between H atoms. Overall, when considering single channel deployment of hydrogen atoms, the loss in adsorption energy is largely related to electrostatic repulsion, i.e., H–H interatomic distances (see Table 1); the H–H distance should not fall below 3 Å. We also considered two cases where two hydrogen atoms are close but situated within two adjacent [001] channels separated by one (110) or (1-10) wall (see Fig. 2 configuration [e] and [f]). If both hydrogen atoms are bonded to distinct oxygen atoms (configuration [e]), the adsorption per H is equivalent to the configuration [c], where repulsive energy almost cancels the chemical binding energies. If the two hydrogen atoms are sharing the same oxygen atom (configuration [f]), the repulsive energy cost is very strong, leading to a positive total energy. This is due to the small distance between H atoms, but also to their charge that is now increased to +0.91 q, making the electrostatic repulsion even more intense. Along the same line, when dealing with an interstitial di-hydrogen molecule in bulk, we observe spontaneous dissociation, leading to the formation of two OH species close to each other, with a positive energy of interaction of 0.27 eV/H and a configuration equivalent to that in configurations [a]. As a first conclusion, H migration and agglomeration will be limited by the electrostatic repulsion, whose effect will become prohibitive if H atoms have to share oxygen atoms along their migration paths. We tested higher hydrogen concentrations along the [001] row, taking advantage of the energy gain supported by configuration [b] (more compact than the configuration [d], even though slightly less energetic). Results indicate that agglomeration is favored, up to the completion of the oxygen row. This gives a filling capability of one H per $RuO_2$ along one single [001] channel. The repulsion observed for hydrogen positioned in adjacent channels will severely restrict further local agglomeration along other directions.

### 3.2. Migration of hydrogen atoms in bulk $RuO_2$

In this section, a systematic determination of activation barriers for hydrogen is performed. We have considered all elementary migrations that allow to further derive all migration paths and calculate diffusion coefficients in bulk $RuO_2$. The adsorbed hydrogen on any of the oxygen atoms can potentially migrate to eight neighbors. Excluding symmetric positions, we end up with five sites: O-A, O–B, O–C, O-D and O-E, shown in Fig. 1-b including their initial and final sites. The corresponding activation barriers and diffusion coefficients are reported in Table 3, with calculation parameters shown in Table 4.

An intrinsic property of $RuO_2$ structure is that it is made of adjacent square “channels” of 3.16 Å side along [110] and [1–10], elongated in the [001] direction (see Fig. 1-a). For sake of clarity, hydrogen atoms and O–H bonds are not represented in Fig. 1-b, but H atoms are labelled in the text by an index that refers to the oxygen atom to which they are bonded. We distinguish intra-channel migration pathways, namely paths $H_O$ - $H_B$, $H_O$ - $H_C$ and $H_O$ - $H_D$, from inter-channel pathways, namely $H_O$ - $H_A$ and $H_O$ - $H_E$ (see Fig. 1-b). The oxygen-to-oxygen distances for O-A, O–B, O–C, O-D and O-E are 2.54 Å, 2.76 Å, 3.24 Å, 3.06 Å and 3.8 Å, respectively. For long-range diffusion possibilities, oxygen to oxygen distances are more relevant than hydrogen hopping distances, since the exact positions of hydrogen atoms provide only local information. The three intra-channel migration pathways are either in a (110) plane ($H_O$ - $H_C$), or

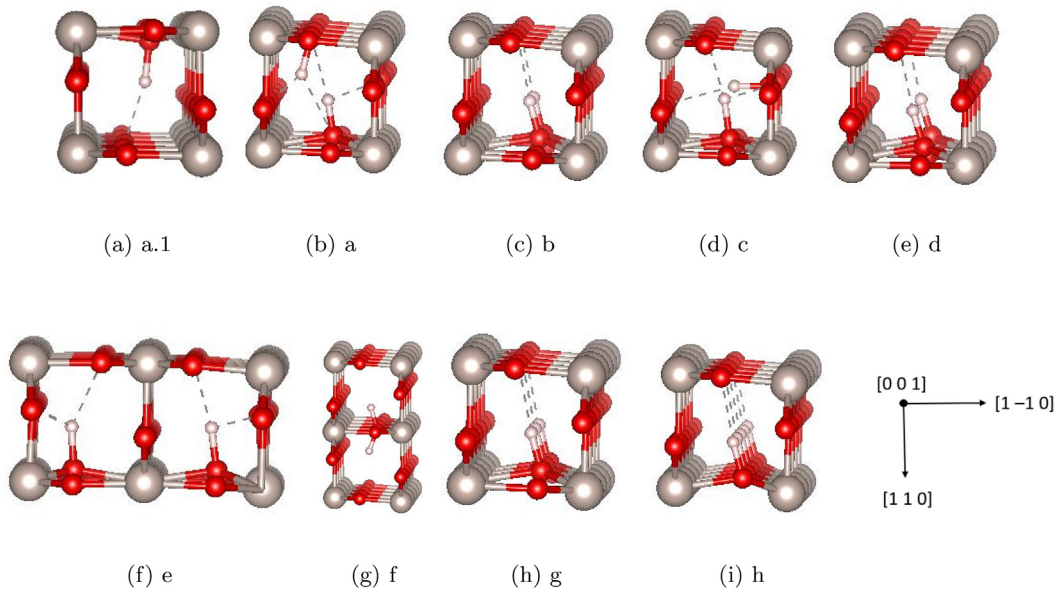


**Fig. 2.** Adsorption configurations of n hydrogens (n = 1, 2, 3, 4) in bulk $RuO_2$. The images show geometry after optimization. [a.1] single atomic hydrogen [a] dissociation of di-hydrogen molecule resulting in two OH species; adsorption of two hydrogen atoms on: [b] adjacent oxygen atoms, OH bond pointing towards [110] direction; [c] one OH pointing towards [110] and the other towards [110]; [d] on alternate oxygen atoms, both OH pointing towards [110]; [e] in neighboring channels, both OH pointing towards [110]; [f] on top and bottom of the same oxygen; [g] 3 hydrogen atoms adsorbed on the row, all OH pointing towards [110]; [h] 4 hydrogen atoms on the oxygen row. *Red*: O; *gray*: Ru; *pink*: H. (For interpretation of the references to colour in this figure legend, the reader is referred to the web version of this article.)

**Table 2**
Agglomeration of hydrogen atoms in bulk $RuO_2$.

| Configuration | Number of H | E(ads)/H, eV | H–H distance, Å | Bader charge on H |
|---|---|---|---|---|
| a.1 | 1 | −0.11 | – | +0.63 |
| a | 2 | 0.27 | 1.07 | +0.62 |
| b | 2 | −0.14 | 3.13 | +0.66 |
| c | 2 | −0.02 | 1.51 | +0.65 |
| d | 2 | −0.17 | 6.16 | +0.65 |
| e | 2 | −0.01 | 2.70 | +0.63 |
| f | 2 | 0.93 | 1.78 | +0.91 |
| g | 3 | −0.20 | 3.08 | +0.65 |
| h | 4 | −0.20 | 3.08 | +0.65 |

**Table 3**
Energy barriers and diffusion coefficients for various hydrogen migration paths in bulk $RuO_2$.

| Pathway | Energy barrier, eV | Diffusion coefficient, $m^2.s^{-1}$ |
|---|---|---|
| O–B | 0.27 | $1.28 \times 10^{-10}$ |
| O–C | 0.28 | $1.82 \times 10^{-10}$ |
| O-D | 0.26 | $1.08 \times 10^{-10}$ |
| O-A: direct pathway | 1.71 | $1.24 \times 10^{-34}$ |
| O-E, 3-steps | | $5.37 \times 10^{-38}$ |
| *i.* O–B | 0.27 | |
| *ii.* Rotation around B | 1.90 | |
| *iii.* B′-E | 0.27 | |

**Table 4**
Vibrational frequencies, hopping distances and diffusion coefficient prefactors for various hydrogen migration paths in bulk $RuO_2$.

| Direction | Frequency, $\nu$, THz | Hopping distance, a, Å | Prefactor, $D_0$, $m^2.s^{-1}$ |
|---|---|---|---|
| [001] | 28.98 | 3.06 | $2.7 \times 10^{-6}$ |
| [110] | 94.61 | 3.24 | $9.9 \times 10^{-6}$ |
| [110] | 32.80 | 3.80 | $4.7 \times 10^{-6}$ |

show a zigzag form with a progression along [001] ($H_O$ - $H_B$ and $H_O$ - $H_D$). $H_O$ - $H_C$ migration is a local move and does not lead to long-range diffusion, since it results in no progression along [001], and it does not allow crossing the channel. For inter-channel migrations, $H_O$ - $H_A$ pathway is a direct curve line from O to A, while $H_O$ - $H_E$ is a three steps pathway including two intra-channel migrations ($H_O$ - $H_B$ and $H_O$ - $H_E$ in two adjacent channels) and a rotation of the hydrogen atom around B taking place at the channels separation facet.

In Table 3, it can be seen that intra-channel pathways exhibit low and similar activation barriers, i.e. steps $H_O$ - $H_B$, $H_O$ - $H_C$ and $H_O$ - $H_D$, requiring about 0.3 eV energy. We can conclude that the intra-channel movements can take place even at room temperature. Nevertheless, these movements will be highly influenced by the agglomeration of hydrogen atoms, and depend on its concentration within each channel, as can be seen from the energetic study presented in section 4.1. In contrast, the two inter-channel migrations, $H_O$ - $H_A$ and $H_O$ - $H_E$, require significantly higher energies, beyond 1.7 eV, which are prohibitive at room temperature and might act as a severe limiting step to hydrogen agglomeration within the crystal matrix. The main lines of these results agree well with those reported in the literature ([41]): intra-channel $H_O$ - $H_B$ and $H_O$ - $H_C$, direct inter-channel $H_O$ - $H_A$ and the rotation around B. An intra-channel migration with a cost of 0.79 eV was calculated in Ref. [15], higher than our 0.3 eV for $H_O$ - $H_D$. To find the source of this discrepancy, we performed a NEB calculation imposing a straight-line migration path between the two sites O and D (see Fig. 4 and we observed a barrier of 0.77 eV which is comparable with the result by Ozolins et al. We conclude the existence of a pathway curved towards the oxygen labelled B, illustrated in Fig. 3, with a much lower energy barrier of 0.26 eV. The presence of a nearby oxygen during H migration prevents the complete breakage of the O–H bond before migration, as observed during the straight-line migration. At the same time, a new O–H bond is now formed with the oxygen in B, as in the O–B case of Table 3. To summarize, we find three migration paths, represented in Fig. 3, between $H_O$ and $H_D$: a two-step path ($H_O$ - $H_B$ followed by $H_B$ - $H_D$), a direct curved path and a straight-line path, also reported in Ref. [15].

Only the two first paths are activated at room temperature. A more detailed analysis of bulk migration was proposed by Kim et al. [18], using

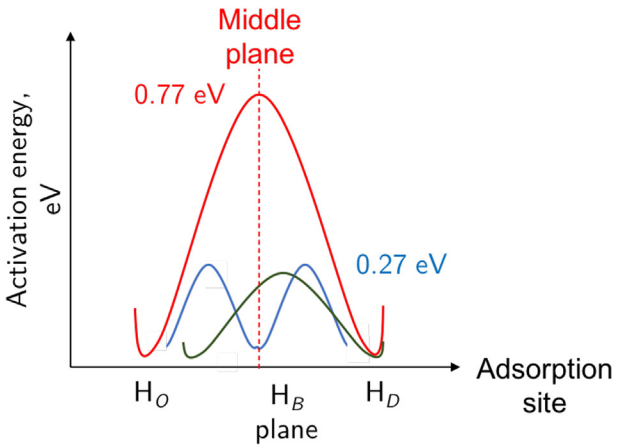


**Fig. 3.** Energy barrier corresponding to $H_O$, $H_B$, and $H_D$ migration. It can be seen that a direct pathway from $H_O$ to $H_D$ costs 0.77 eV energy, however, a two-steps pathway is energetically cheaper.

a single unit cell associated to a fine mesh of k points. Their results are in agreement with our data (Table 3) where the migrations along [001] are effective at room temperature. Discrepancies arise for high activation barriers, along [110], where hydrogen diffusion is only effective at very high temperature. The source of discrepancy is probably due to the small size of the cell used in Ref. [41], which introduces electrostatic interaction between very close ionized hydrogen atoms when applying periodic boundary conditions. Finally, the $H_O$ - $H_B$ type migrations, whose combination will lead to an effective $H_O$ - $H_E$ zigzag migration path along [001] (see Table 3 and Fig. 3), has not been investigated in the literature. The values of the diffusion coefficients are reported in Table 3. They are calculated according to the Arrhenius law:

$$D = D_0\, exp(-\Delta E / K_B T). \tag{2}$$

$D_0$ is the prefactor determined using the vibration frequency, $\nu$ and the hopping distance a as $D_0 = \nu a^2$. The vibration frequencies are extracted from the phonon spectrum of bulk $RuO_2$. $\Delta E$ is the activation barrier determined with NEB calculations, $K_B$ the Boltzmann constant and T the temperature (values given in Table 4).

## 4. Surface $RuO_2$

The $RuO_2$-(110) surface is very well-documented experimentally and theoretically [4,8,17–21,25,42–47], because of catalytic properties of $RuO_2$, mostly for dehydrogenation. Two types of (110) surface have been studied. For the first type (see Fig. 5), the surface is composed of unsaturated Ru species (noted $Ru_{cus}$) presenting one missing oxygen atom, resulting in a dangling bond normal to the surface, and one row of bridging oxygen atoms (noted $O_{br}$) located on top of ruthenium rows. In addition, the surface also exhibits in plane saturated oxygen atoms, i.e. bonded to three ruthenium atoms (noted $O_{pl}$, see Refs. [6,7,20,45] for details on this surface). The other type of surface is documented to a lesser extent. It consists in an oxygen rich surface, similar in all points to that represented in Fig. 5, except that one additional oxygen atom is now present on top of each $Ru_{cus}$ surface atom [6,7,20,45]. The focus of studies on this latter surface is rather sparse. They concern CO reaction [20], water deprotonation [45], and oxygen evolution reaction [45] (see Fig. 6).

Only two contributions were found on the interaction with $H_2$ in the perspective of further water formation on the surface and further reaction with other molecular species such as CO, $CO_2$, $NH_3$ [7,20]. The contribution by Zhan et al. [6] is the only one related to pseudo-capacitance investigations. It focuses more on the determination of the capacitance value on predefined surface configurations rather than on the underlying mechanisms leading to these configurations. For what concerns hydrogen interaction specifically, the body of the literature is dedicated to the splitting of dihydrogen at low temperature onto the first type of (110) surface, in which DFT calculations are mostly supporting ultra-high vacuum imaging and temperature programmed desorption experiments [17,21,25]. For that reason, in the following text, we will concentrate our effort on the first type of (110) surface. Before addressing surface agglomeration and migration of hydrogen, we start by calculating the adsorption energy of both molecular and atomic hydrogen on all surface sites. Atomic adsorption is often omitted in the literature that focuses exclusively on $H_2$ interacting with catalytic surface sites, namely $O_{br}$ and $Ru_{cus}$ sites. However, in some applications, like capacitors, the hydrogen is preferentially displayed in atomic form, for instance via protic liquids or HCl medium, and the interest resides in its capability to adsorb/desorb, migrate and agglomerate on the substrate, making the approach slightly different from catalysis experimental or theoretical perspective.

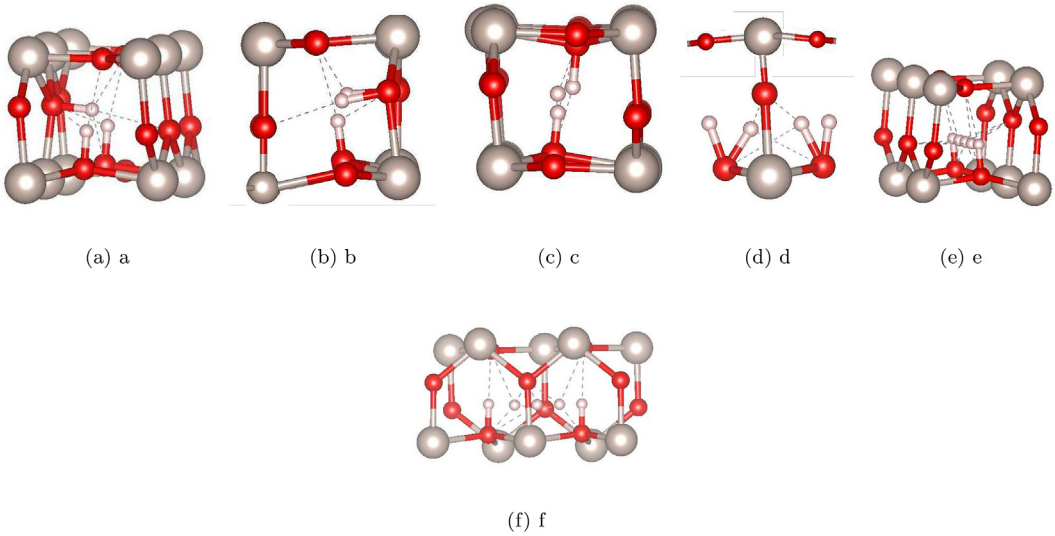


**Fig. 4.** The three inter-channel migration of hydrogen, along the path [a] O-D [b] O–B [c] O–C and one intra-channel pathway [d] A-O in bulk $RuO_2$. Figure [d] shows the intra-channel migration of hydrogen along the path O-A in bulk $RuO_2$. Figures [e, f] show two different views of the constrained pathway of a hydrogen atom, along O-D, in bulk $RuO_2$.

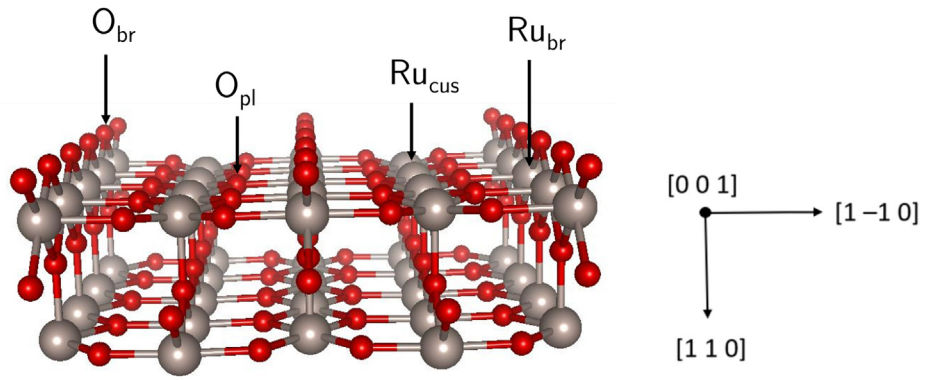


**Fig. 5.** A schematic diagram showing the $RuO_2$ (110) surface model. *Red*: planar oxygen $O_{pl}$; *blue*: bridging oxygen $O_{br}$; *gray*: Ru. (For interpretation of the references to colour in this figure legend, the reader is referred to the web version of this article.)

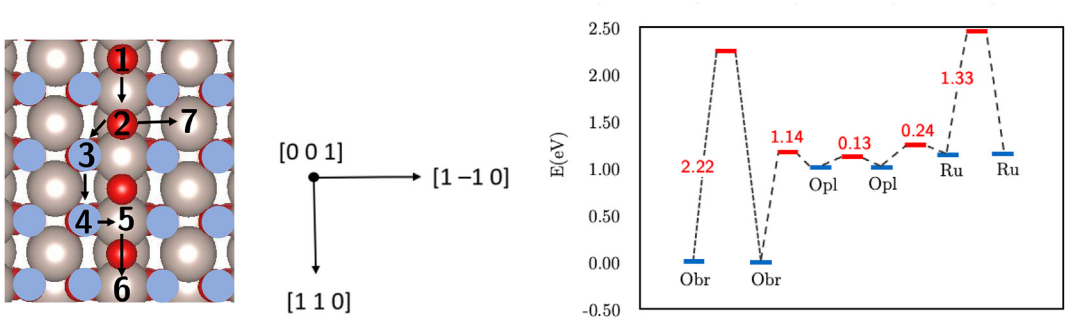


(a) a (c) b

**Fig. 6.** [a] Top view of potential migration paths of a hydrogen atom on $RuO_2$ surface and associated energy barriers. [b] Energy profile associated with surface migration of a hydrogen atom on $RuO_2$ (110) surface; adsorption of H on $O_{br}$ is taken as reference here. *Red*: planar oxygen $O_{pl}$; *blue*: bridging oxygen $O_{br}$; *gray*: Ru. (For interpretation of the references to colour in this figure legend, the reader is referred to the web version of this article.)

### 4.1. Adsorption of molecular and atomic hydrogen on $RuO_2$ (110)

Adsorption energies analysis for isolated H atom and $H_2$ are given in Table 5. For atomic hydrogen, the most stable position is on top of $O_{br}$ sites with an adsorption energy of −0.95 eV. This energy is substantially higher compared to the adsorption energy in bulk which is −0.11 eV. The adsorption on $O_{pl}$ and on Ru remains, by far, thermodynamically less favorable. The least favorable case corresponds to the hydrogen on top of the ruthenium atom, +0.20 eV. The quantitative values match correctly with previously reported data. However, they are all obtained at higher coverage (1 and 0.5 ML), which explains the slight deviations [21,25,26]. Note that our reported values are obtained for 0.125 ML. Table 5 contains some of these higher coverage data for rough comparison. The work by Wei et al. investigated our coverage for the cus site, giving a value of −0.40 eV which is in the mid range between our calculated value (−0.48 eV) and the full coverage value −0.32 eV. Overall, the differences, notably for both the $Ru_{cus}$ site and the water like structure obtained for the dissociated form of dihydrogen on top of $O_{br}$, is related to the fact that adsorption is shown to be coverage dependent, as reported by all studies in literature. For interesting details on the charge transfers, geometrical and vibrational frequency analysis of these configurations, we refer the reader to Ref. [25]. Notice that $O_{pl}$ has never been discussed in depth. Our calculations show that it has roughly no interaction with hydrogen (close to 0 eV in Table 5), in rough agreement with data from Wei et al., which in contrast, have more stable value for low coverages. We will show that this configuration can still play a non negligible role on migration, as we will see in section 5.3. Dihydrogen adsorption and reaction on the (110) surface has been the subject of detailed research to picture the fundamentals of $RuO_2$ catalytic activity. While there is still some debate on the adsorption and dissociation at very low temperatures (5 K), there is general consensus on that $Ru_{cus}$ sites only can afford adsorption of $H_2$ in molecular form. We calculated the adsorption energy of a dihydrogen molecule on top of $Ru_{cus}$ to be −0.48 eV (the distance between $H_2$ and surface $Ru_{cus}$ is 1.87 Å, and H–H bond length is 0.80 Å). This is in agreement with values of the literature, where adsorption energy is shown to be coverage dependent, with a drop in energy down to −0.32 eV at full $Ru_{cus}$ coverage. This is a counter intuitive result with respect to atomic hydrogen adsorption, calculated to be positive on this site (see Table 5). The exact nature of this molecular bonding is well described in Ref. [25], where we also learn that the potential hyper-surface at this configuration allows for a quasi free rotation (0.1 eV activation) of the molecule around its [110] symmetry axis, associated with a flat potential hypersurface towards the $O_{br}$ axis explaining how dissociation may occur as observed experimentally. On the $O_{br}$ site, only a dissociated form is obtained, with −0.95 eV (comparable to the value by Sun et al. [25] obtained at higher coverage). But the relation with experiment show that the barrier for direct dissociation on this site is unlikely. Experimentally,

**Table 5**
Adsorption energies of atomic and molecular hydrogen on $RuO_2$ surface, on different sites for 0.125 ML; WL: water like structure; ML: monolayer.

| Ads. site | $E_{ads}$ H (eV) | $E_{ads}$ $H_2$ (eV) | H [25,26]; | $H_2$ [25,26]; |
|---|---|---|---|---|
| $O_{br}$ | −0.95 | −0.90 (WL) | −0.89; −0.96 (1 ML) | −0.56; −0.70 (0.5 ML, WL) |
| $O_{pl}$ | +0.06 | none | / | none |
| $Ru_{cus}$ | +0.20 | −0.48 | +0.20; /(0.5 ML) | −0.32; −0.36 (1 ML) |

after dissociation at low temperature (less than 90 K), the surface exhibits a configuration with two H monohydrides $Ru_{cus}$-H and $O_{br}$-H. DFT determination of the dissociation path from molecular state on top of $Ru_{cus}$ [21], lead to an activation barrier of 0.22 eV, compatible with dissociation at 90 K. However, the recent study by Dahal et al. [17] unraveled that dissociation can occur as low as 5 K and discussed the potential mechanisms arising during dissociation. They explain that dissociation could be effective despite the high value of the activation barrier at this temperature. We were not able to calculate alternative pathways with lower activation to explain this discrepancy.

### 4.2. Agglomeration of hydrogen atoms on $RuO_2$ (110)

We start by investigating the interaction energy of hydrogen atoms distributed on various surface sites. Adsorption energies per hydrogen atom are reported in Table 6. In contrast to what is observed in bulk, there is no clear evidence of agglomeration propensity of hydrogen atoms on the surface, even though most tested configurations show better stability of agglomerated configurations compared with the formation of molecular hydrogen, due to the relatively high adsorption energy of surface monohydrides on top of $O_{br}$ sites. This means that molecular hydrogen should dissociate in atomic species, but dispersed over the surface. Considering two hydrogen atoms positioned on top of adjacent $O_{br}$ sites, which is the most energetically favorable case of all tested configurations with two hydrogen atoms, there is a loss of 0.05 eV energy per hydrogen atom compared to the isolated monohydride (see Table 6). This loss increases by roughly 0.5 eV if the second hydrogen atom is now positioned on top of the $O_{pl}$ or $Ru_{cus}$ sites. However, this configuration remains still more favorable than $H_2$ on the surface. Note that a dihydride configuration on top of a single $O_{br}$ site has a much lower energy gain, of −0.25 eV/H atom (see Table 5). This dihydride could a priori serve as an intermediate configuration during the dissociation of molecular hydrogen as discussed in Ref. [25]. Saturating two $Ru_{cus}$ or two $O_{pl}$ with the monohydride configuration does not make any energy change compared to the isolated configuration. Increasing now the coverage along the $O_{br}$ row with four hydrogen atoms, which completes a given oxygen row of the unit cell, the endothermal component previously observed for two agglomerated monohydrides on top of $O_{br}$ sites is slightly increased by a few meV. But, the energetic budget remains still largely favorable. Covering all $O_{br}$ sites in our model, i.e. two $O_{br}$ rows, marginally modifies the overall energy gain (additional 0.03 eV agglomeration penalty). Higher hydrogen density on the surface necessitates further adsorption sites than $O_{br}$ sites only. Among all tested configurations, combinations and coverages, only the association of H-saturated $O_{br}$ sites with $Ru_{cus}$ shows overall energy gain upon gas phase molecular hydrogen. It can safely be said that the adsorption is largely dependent on the surface coverage. A schematic diagram showing main tested surface coverages as discussed here is shown in SI (Fig. S2) for better clarity. From the literature, the agglomeration has been treated in a different manner, with increasing a (1 × 1) surface unit, and focusing more on the $O_{br}$ mono and dihydrides, and $Ru_{cus}$ monohydride. The results for adjacent $O_{br}$ and $Ru_{cus}$ fit well with the only one reported value in Ref. [21] (−0.50 eV/H). Most of the other values given in Table 5 do not have exact equivalent in the literature. However, results already discussed above concerning the isolated species, and notably on the $O_{br}$ site with high density, match well with our calculations.

**Table 6**
Agglomeration of hydrogen atoms on $RuO_2$ surface: adsorption sites and corresponding adsorption energies. *D*: dissociated $H_2$; *A*: molecular $H_2$.

| Number of hydrogen atoms | Adsorption sites | Adsorption energy/H (eV) |
|---|---|---|
| 2 | $O_{br}$ and $O_{br}$ (D) | −0.90 |
| | $O_{br}$ and Ru (D) | −0.54 |
| | $O_{br}$ and $O_{pl}$ (D) | −0.48 |
| | $O_{br}$ dihydride | −0.25 |
| | Ru and $O_{pl}$ (D) | 0.054 |
| | Ru and Ru | +0.20 |
| 4 | $O_{br}$ (one row of $O_{br}$) | −0.87 |
| 8 | $O_{br}$ (both rows of $O_{br}$) | −0.85 |
| | Ru (both rows of Ru) | 0.28 |
| 16 | 8.Ru and 8.$O_{br}$ | −0.46 |
| 24 | 8.$O_{br}$ and 16.$O_{pl}$ | 0.73 |
| 32 | 8.Ru and 8.$O_{br}$ and 16.$O_{pl}$ | 0.04 |

### 4.3. Migration of hydrogen atom on $RuO_2$ (110)

Similarly to Section 3.2 addressing migration of isolated hydrogen atom in bulk $RuO_2$, we tested all possible elementary migration steps that hydrogen can afford on the surface. Results are presented in Table 7. It can be seen that the associated energy barrier for direct migration between $O_{br}$ sites is 2.2 eV, which shows that direct migration between the most stable sites for hydrogen is thermodynamically not feasible even at moderate temperatures. However, from the most stable $O_{br}$ sites, hydrogen can move to the $O_{pl}$ sites, with a 1.14 eV energy barrier, this migration can be reasonably expected at moderate temperature. Further, we calculate that the most favorable pathways for hydrogen to move on the surface is from $O_{pl}$ sites to another $O_{pl}$ sites, either along the [001] direction with an associated energy barrier of 0.13 eV, or in the perpendicular [1–10] direction, showing that hydrogen can migrate in all directions on the surface, at room temperature, the most important barrier being to overcome the row of $O_{br}$ oxygen atoms (1.14 eV barrier).

## 5. Hydrogen penetration into the $RuO_2$ subsurface

Until very recently, the behavior of hydrogen into the $RuO_2$ subsurface has not been addressed despite its potential interest for a number of applications, such as corrosion, embrittlement, surface catalysis, in addition to the capability of the surface to reversibly absorb a flux of incoming hydrogen atoms. This latter point is of major importance for energy related applications like storage and harvesting. Bulk results indicate that hydrogen may accumulate to some extent, but the displacement of hydrogen atoms in the crystal matrix is largely anisotropic. In particular migration along the [110] direction exhibits activation superior to 1.7 eV which inhibits any hydrogen mass transfer in this direction. In the following we investigate H penetration into the subsurface to determine whether bulk migration inhibitions may be attenuated in the case of the subsurface, and if so, to which extent in depth. We will also investigate H penetration into $RuO_2$ (001) surface as an alternative to the (110) orientation, as motivated by the bulk [001] migration pathway profile showing high potential for diffusion.

### 5.1. Hydrogen penetration into the $RuO_2$ (110) subsurface

The adsorption of a single hydrogen atom has been discussed in Section 5. From the most stable site, i.e. on top of a bridging oxygen atom, the migration towards the subsurface is shown to be a two-step process. First, the hydrogen will stabilize on top of the $O_{pl}$ site, closer to the saddle point on the way to cross the surface layer. This hopping process, illustrated in Fig. 7[a] (point 1 to point 2), has a calculated energy barrier of 1.14 eV (see Table 7). The second step (point 2 to point 3 in Fig. 7[a]), brings the hydrogen atom to its stable position. There, it is stabilized

**Table 7**
Migration path of a hydrogen atom on $RuO_2$ (110) surface and associated energy barrier. $O_{br}$: bridging oxygen; $O_{pl}$: planar oxygen.

| Migration path (number) | Energy barrier (eV) |
|---|---|
| $O_{br}$ to $O_{br}$ (1 → 2) | 2.22 |
| $O_{br}$ to $O_{pl}$ (2 → 3) | 1.14 |
| $O_{pl}$ to $O_{pl}$ (3 → 4) | 0.13 |
| $O_{pl}$ to Ru (4 → 5) | 0.24 |
| Ru to Ru (5 → 6) | 1.33 |
| $O_{br}$ to Ru (2 → 7) | 1.34 |

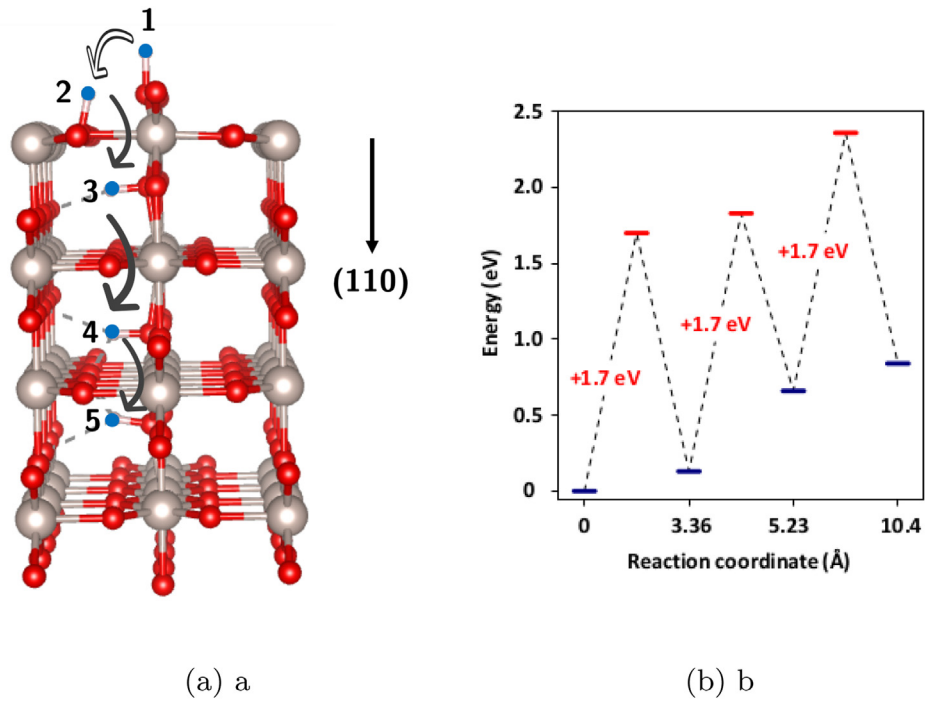


**Fig. 7.** Migration of hydrogen from the surface to sub-surface of $RuO_2$ (110). *Red*: oxygen; *gray*: Ru; *blue*: proton. (For interpretation of the references to colour in this figure legend, the reader is referred to the web version of this article.)

exactly in the configuration of the unique bulk adsorption site. Its energy level (−0.85 eV) is much lower compared to the bulk value (−0.11 eV), although slightly higher than on the (110) surface (−0.95 eV). This indicates that thermodynamically, the subsurface is largely preferred to bulk position. However, the migration, with an activation barrier of 1.7 eV, is kinetically prohibited at ambient or moderate temperature. It should be noticed that alternate cavities along [110] direction are similar, in terms of structural configuration, but not for migration. This mechanism was described in section 3, where we observed two migration paths along [110]: direct HO-HA and three-step rotational HO-HE (see Table 3). In Fig. 7[a], migration of a hydrogen from point 2 to point 3, would follow the direct pathway. However, from point 3 to 4, the hydrogen will 'feel' the effect of Ru as point 3 to 4 is not a direct pathway but the rotational pathway. This pattern of alternate direct and rotational pathways is repeated as we go deeper along [110] direction. Near the surface, the calculated energy barrier from point 2 to 3 is 1.7 eV, the same as in bulk. Furthermore, the barrier to go from point 3 to 4, which is a rotational pathway, is also 1.7 eV, compared to 1.9 eV in deep bulk. Due to surface effects, this barrier is reduced by 0.2 eV. Moving on, the barrier from 4 to 5, a direct pathway, is again 1.7 eV. The energy profile associated with hydrogen penetration is shown in Fig. 7[b].

### 5.2. *Hydrogen penetration into the $RuO_2$ (001) subsurface*

The $RuO_2$ (001) surface was modelled by cleaving the bulk along (001) direction. Cleaving the bulk results in a plane surface which has both Ru and O atoms on the surface, see Fig. 8. Fig. 8 [a] shows a top view of the (001) surface where three different sites considered for H adsorption are marked. The adsorption energies are presented in Table 8. The adsorption on $RuO_2$ (001) follows the same trend as $RuO_2$ (110) with the most stable site being $O_{br}$ and the least stable being on top of Ru. However, the adsorption is less favored compared with $RuO_2$ (110).

Fig. 8 [b] shows a front view of $RuO_2$ (001) where elementary steps of the penetration of a H atom from the surface to the subsurface is shown and elementary steps are provided. A hydrogen atom is stabilized on $O_{br}$ in the first cavity with an adsorption energy of −0.24 eV. In the third cavity, the adsorption energy is −0.12 eV, and we can consider to have reached the bulk regime. The energy barrier from $O_{br}$ to $O_{pl}$ on the surface is 0.22 eV. A hydrogen atom diffuses from $O_{pl}$ of the surface to $O_{pl}$ at the bottom of the first cavity, with an energy barrier of 0.43 eV. The third jump, from the first cavity to the second mimics the bulk regime, with an energy barrier of 0.26 eV. The energetic profile is shown in Fig. 8[c].

The significantly lower energy barrier (0.43 eV, compared with 1.7 eV for $RuO_2$ (110)) for penetration of a hydrogen atom in subsurface opens doors for $RuO_2$ (001) oriented surface applications in fields such as pseudocapacitance. $RuO_2$ (001) thin films can be engineered which will allow easy pathways for penetration of hydrogen atoms in the subsurface hereby giving enhanced efficiencies.

## 6. Conclusions

We have reviewed and investigated the interaction of hydrogen (molecular as well as in atomic form) with $RuO_2$ (110) oriented surface. We investigated bulk $RuO_2$, the $RuO_2$ (110) surface, and importantly, the subsurface region which a priori possesses specific properties which remained unanswered in literature. Our calculations include hydrogen energetics as well as the spatial extension of the particular transition region between surface and bulk $RuO_2$, which we call subsurface. We systematically provided adsorption energies, capability for hydrogen to agglomerate, and derived diffusion constants from activation barriers and vibrational properties. We first conclusively show that adsorbed atomic hydrogen on all tested regions exhibits a proton like behavior due to the large depletion of its electronic density when it interacts with oxygen atoms (+0.63 q). Hydrogen in bulk can agglomerate within the [001] oriented channels at the level of (0.01H/Å $^3$, in a single channel). We demonstrate that the electrostatic repulsion caused by its positive charge limit agglomeration across adjacent channels. We determined migration pathways from which diffusion coefficients were derived, showing great anisotropy of hydrogen migration in bulk ([001] largely favored). On the surface, hydrogen adsorption is shown to be coverage

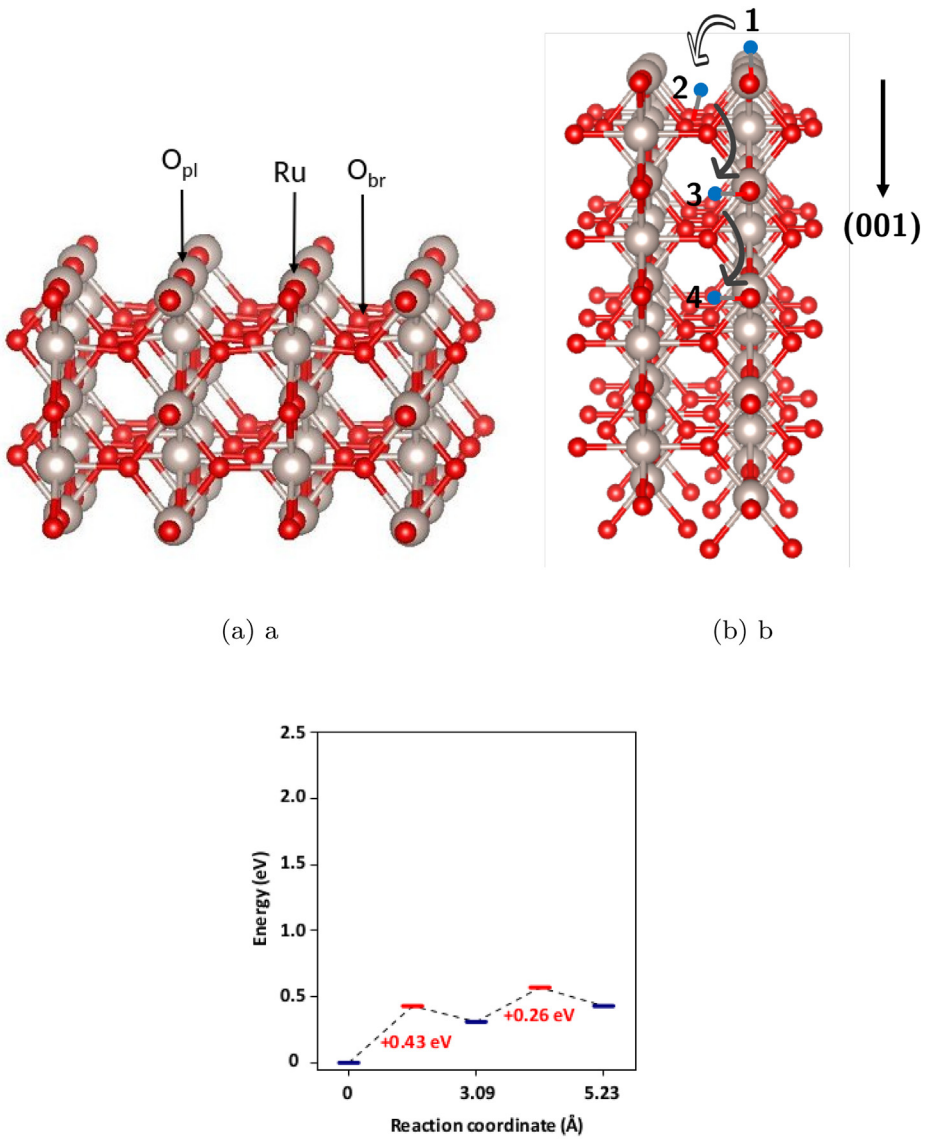


**Fig. 8.** [a] View of $RuO_2$ (001) surface [b] migration of a proton from the surface to sub-surface of $RuO_2$ (001) [c] calculated energy barrier for penetration. *Red*: oxygen; *gray*: Ru; *blue*: hydrogen. (For interpretation of the references to colour in this figure legend, the reader is referred to the web version of this article.)

**Table 8**
Adsorption energies of atomic hydrogen on $RuO_2$ (001) surface, at different sites.

| Adsorption site | $E_{ads}$, eV (for H) |
|---|---|
| $O_{br}$ | −0.55 |
| $O_{pl}$ | +0.12 |
| Ru | +0.17 |

dependent, but the agglomeration is shown to be driven by adsorption rather than electrostatic repulsion. The saturation of all surface $O_{br}$ sites is feasible, in addition to which $Ru_{cus}$ sites can be also saturated, giving a hydrogen surface density of 0.1 H/Å $^3$. We finally investigated the sub-surface region. Its spatial extension, where hydrogen energetics is different from both bulk and surfaces, is of 10.4 Å in depth. While adsorption energies are rather high compared to the bulk in this region, activation barriers for migration are not affected. With 1.7 eV barrier, this makes penetration unfeasible at the ambient temperature, in the absence of an electrical field. Here, hydrogen penetration is much easier, with a maximum of 0.43 eV barrier for over passing the surface layer. Its spatial extension necessary to reach bulk properties, where easy [001] migration is calculated, is shortened to 5.2 Å.

## CRediT authorship contribution statement

**Ankita Jadon:** Conceptualization, Methodology, Data curation, Writing – original draft, preparation, Writing – review & editing, Visualization, Investigation. **Carole Rossi:** Supervision. **Mehdi Djafari-Rouhani:** Conceptualization, Methodology, Data curation, Writing – original draft, preparation, Writing – review & editing, Visualization, Investigation, Supervision. **Alain Estève:** Conceptualization, Methodology, Data curation, Writing – original draft, preparation, Writing – review & editing, Visualization, Investigation, Supervision. **David Pech:** Supervision.

## Declaration of competing interest

The authors declare that they have no known competing financial interests or personal relationships that could have appeared to influence the work reported in this paper.

## Acknowledgements

We acknowledge the support from the European Research Council (ERC, Consolidator Grant, ERC-2017-CoG, Project 771793 3D-CAP). This work was granted access to the high-performance computing resources of CALMIP supercomputing center.

## Appendix A. Supplementary data

Supplementary data to this article can be found online at https://doi.org/10.1016/j.physo.2021.100059.

## References

[1] U.A. Paulus, Y. Wang, S.H. Kim, P. Geng, J. Wintterlin, K. Jacobi, G. Ertl, Inhibition of CO oxidation on RuO 2(110) by adsorbed H 2O molecules, J. Chem. Phys. (2004) 3–4.
[2] Qing Li, Shasha Zheng, Yuxia Xu, Huaiguo Xue, Huan Pang, Ruthenium Based materials as Electrode materials for supercapacitors, 2018.
[3] Theresa Sperger, Italo A. Sanhueza, Franziska Schoenebeck, Computation and experiment: a powerful combination to understand and predict reactivities, Accounts Chem. Res. 49 (6) (2016) 1311–1319.
[4] Manh Thuong Nguyen, Rentao Mu, David C. Cantu, Igor Lyubinetsky, Vassiliki Alexandra Glezakou, Zdenek Dohn\\'alek, Roger Rousseau, Dynamics, stability, and adsorption states of water on oxidized RuO2(110), J. Phys. Chem. C (2017) 2.
[5] Reshma R. Rao, Manuel J. Kolb, Jonathan Hwang, Filsøe Pedersen Anders, Apurva Mehta, Hoydoo You, Kelsey A. Stoerzinger, Zhenxing Feng, Hua Zhou, Hendrik Bluhm, Livia Giordano, Ifan E.L. Stephens, Yang Shao-Horn, Surface orientation dependent water dissociation on rutile ruthenium dioxide, J. Phys. Chem. C (2018) 1–3.
[6] Cheng Zhan and De-En Jiang. reportUnderstanding the Pseudocapacitance of RuO 2 from Joint Density Functional Theory. Technical report.
[7] Yinying Wei, Umberto Martinez, Lutz Lammich, Flemming Besenbacher, Stefan Wendt, Atomic-scale view on the H2O formation reaction from H2 on O-Rich RuO2(110), J. Phys. Chem. C 118 (48) (12 2014) 27989–27997.
[8] H. Over, Y.D. Kim, A.P. Seitsonen, S. Wendt, E. Lundgren, M. Schmid, P. Varga, A. Morgante, G. Ertl, Atomic-scale structure and catalytic reactivity of the RuO2(110) surface, Science (2000) 2–4.
[9] S.N. Pusawale, P.R. Deshmukh, P.S. Jadhav, C.D. Lokhande, Electrochemical properties of chemically synthesized SnO2-RuO2 mixed films, Mater. Renew. Sustain. Energy 8 (1) (2019) 3.
[10] Bulk-and-surface-electronic-structure-of-Lisub2subO_1996_Physical-Revie w-B—Condensed-Matter-and-Materials-Physics.
[11] W. Lonsdale, M. Wajrak, K. Alameh, Manufacture and application of RuO2 solid-state metal-oxide pH sensor to common beverages, Talanta (2018).
[12] Jin Kim Su, Hayoung Jung, Chongmok Lee, Myung Hwa Kim, Youngmi Lee, Biological application of RuO2 nanorods grown on a single carbon fiber for the real-time direct nitric oxide sensing, Sensor. Actuator. B. Chem. (2014) 2.
[13] Takashi Hibino, Kazuyo Kobayashi, Masahiro Nagao, Yuta Yamamoto, Design of a rechargeable fuel-cell battery with enhanced performance and cyclability, J. Electrochem. Soc. 163 (7) (2016) A1420–A1428.
[14] Amod Kumar, Vijay K. Ramani, RuO2-SiO2 mixed oxides as corrosion-resistant catalyst supports for polymer electrolyte fuel cells, Appl. Catal. B Environ. (2013) 1–2.
[15] Yongduo Liu, Fei Zhou, Vidvuds Ozolins, Ab initio study of the charge-storage mechanisms in RuO 2-based electrochemical ultracapacitors, J. Phys. Chem. C 116 (1) (2 2012) 1450–1457.
[16] Pawel Pomorski, Lars Pastewka, Christopher Roland, Hong Guo, Jian Wang, Capacitance, induced charges, and bound states of biased carbon nanotube systems, Phys. Rev. B 69 (11) (2004) 115418, 2.
[17] Arjun Dahal, Rentao Mu, Igor Lyubinetsky, Zdenek Dohn\\'alek, Hydrogen adsorption and reaction on RuO2(110), Surf. Sci. 677 (2 2018) 264–270.
[18] Y.D. Kim, A.P. Seitsonen, S. Wendt, J. Wang, C. Fan, H. K Jacobi, Over, and G Ertl. Characterization of various oxygen species on an oxide surface: RuO2(110), J. Phys. Chem. B (2001) 3–6.
[19] Rentao Mu, David C. Cantu, Vassiliki Alexandra Glezakou, Igor Lyubinetsky, Roger Rousseau, Zdenek Dohn\\'alek, Deprotonated water dimers: the building blocks of segmented water chains on rutile RuO2(110), J. Phys. Chem. C (2015) 2–4.
[20] K. Jacobi, Y. Wang, G. Ertl, Interaction of hydrogen with RuO2(110) surfaces: activity differences between various oxygen species, J. Phys. Chem. B (2006) 2–6.
[21] Yinying Wei, Umberto Martinez, Lutz Lammich, Flemming Besenbacher, Stefan Wendt, Formation of metastable, heterolytic H-pairs on the RuO2(110) surface, Surf. Sci. (2014) 2–4.
[22] M. Knapp, D. Crihan, A.P. Seitsonen, A. Resta, E. Lundgren, J.N. Andersen, M. Schmid, P. Varga, H. Over, Unusual process of water formation on RuO2(110) by hydrogen exposure at room temperature, J. Phys. Chem. B (2006) 4–6.
[23] Jinhai Wang, Chao Yang Fan, Qiang Sun, Karsten Reuter, Karl Jacobi, Matthias Scheffler, Gerhard Ertl, Surface coordination chemistry: dihydrogen versus hydride complexes on RuO2(110), Angew. Chem. Int. Ed. 42 (19) (5 2003) 2151–2154.
[24] Rentao Mu, David C. Cantu, Xiao Lin, Vassiliki Alexandra Glezakou, Zhitao Wang, Igor Lyubinetsky, Roger Rousseau, Zdenek Dohn\\'alek, Dimerization induced deprotonation of water on RuO2(110), J. Phys. Chem. Lett. (2014) 2–5.
[25] Qiang Sun, Karsten Reuter, Matthias Scheffler, Hydrogen adsorption on RuO2(110): density-functional calculations, Phys. Rev. B Condens. Matter (2004) 4.
[26] M. Knapp, D. Crihan, A.P. Seitsonen, E. Lundgren, A. Resta, J.N. Andersen, H. Over, Complex interaction of hydrogen with the RuO2(110) surface, J. Phys. Chem. C (2007) 2–5.
[27] Young-Min Kim, In-Ho Jung, Byeong-Joo Lee, Atomistic modeling of pure Li and Mg–Li system, Model. Simulat. Mater. Sci. Eng. 20 (3) (2012) 35005.
[28] Vidvuds Ozoliņš, Fei Zhou, Mark Asta, Ruthenia-based electrochemical supercapacitors: insights from first-principles calculations, Accounts Chem. Res. 46 (5) (5 2013) 1084–1093.
[29] Ankita Jadon, et al., Rethinking Pseudocapacitance: A Way to Harness Charge Storage of Crystalline $RuO_2$, ACS Appl. Energy Mater. (2020), https://doi.org/10.1021/acsaem.0c00476. In press.
[30] W. Kohn and L. J. Sham. Self-consistent equations including exchange and correlation effects. Phys. Rev., 140(4A), 1965.
[31] D. Joubert, From ultrasoft pseudopotentials to the projector augmented-wave method, Phys. Rev. B Condens. Matter 59 (3) (1999) 1758–1775.
[32] Jürgen Hafner, ¡i¿Ab-initio¡/i¿ simulations of materials using VASP: density-functional theory and beyond, J. Comput. Chem. 29 (13) (2008) 2044–2078, 10.
[33] Jiří Klimeš, Angelos Michaelides, Perspective : Advances and challenges in treating van der Waals dispersion forces in density functional theory Perspective : Advances and challenges in treating van der Waals dispersion, 2012, 120901.
[34] S. Grimme, J. Antony, S. Ehrlich, H. Krieg, A consistent and accurate ab initio parametrization of density functional dispersion correction (DFT-D) for the 94 elements H-Pu, J. Chem. Phys. 132 (15) (2010).
[35] M. Methfessel, A.T. Paxton, High-precision sampling for Brillouin-zone integration in metals, Phys. Rev. B 40 (6) (1989) 3616–3621.
[36] Y.D. Kim, A.P. Seitsonen, S. Wendt, J. Wang, C. Fan, H. K Jacobi, Over, and G Ertl. Characterization of various oxygen species on an oxide surface: RuO2(110), J. Phys. Chem. B (2001) 2–3.
[37] Yavar T. Azar, Mahmoud Payami, First-Principles Calculation of Electronic Energy Level Alignment at Electrochemical Interfaces, 2017, p. 1.
[38] Peter Davies, Energy Storage at Perovskite Interfaces, Technical report, 2018.
[39] G. Henkelman, A. Arnaldsson, H. Jónsson, A fast and robust algorithm for Bader decomposition of charge density, Comput. Mater. Sci. 36 (3) (2006) 354–360.
[40] Samuel Kim, Wensheng Lai, Hydrogen diffusion behavior and vacancy interaction behavior in OsO2and RuO2by ab initio calculations, Comput. Mater. Sci. (2015) 1–4.
[41] Samuel Kim, Wensheng Lai, Hydrogen diffusion behavior and vacancy interaction behavior in OsO2 and RuO2 by ab initio calculations, Comput. Mater. Sci. (2015) 1–2.
[42] Karsten Reuter, Matthias Scheffler, Composition , structure , and stability of RuO 2 110 … as a function of oxygen pressure 65 (December) (2001) 1–11.
[43] Qiang Sun, Karsten Reuter, Matthias Scheffler, Effect of a Humid Environment on the Surface Structure of RuO2(110), vol. 2, 2003. July.
[44] Sampyo Hong, S Rahman Talat, Karl Jacobi, Gerhard Ertl, Interaction of NO with RuO2(110) surface: a first principles study, J. Phys. Chem. C (2007) 2–4.
[45] Reshma R. Rao, Manuel J. Kolb, Niels Bendtsen Halck, Filsøe Pedersen Anders, Apurva Mehta, Hoydoo You, Kelsey A. Stoerzinger, Zhenxing Feng, Heine A. Hansen, Hua Zhou, Livia Giordano, Jan Rossmeisl, Tejs Vegge, Ib Chorkendorff, Ifan E.L. Stephens, Yang Shao-Horn, Towards identifying the active sites on RuO2(110) in catalyzing oxygen evolution, Energy Environ. Sci. (2017) 3–4.
[46] H. Over, Y.D. Kim, A.P. Seitsonen, S. Wendt, E. Lundgren, M. Schmid, P. Varga, A. Morgante, G. Ertl, Atomic-scale structure and catalytic reactivity of the RuO2(110) surface, Science (2000) 3–5.
[47] Karsten Reuter, Matthias Scheffler, Composition, structure, and stability of (formula presented) as a function of oxygen pressure, Phys. Rev. B Condens. Matter 65 (3) (2002) 1–11.